Intercomparison of the Southern Ocean Circulations in IPCC Coupled Model Control Simulations

By Joellen L. Russell[1], Ronald J. Stouffer[2] and Keith W. Dixon[2]

1) **Atmospheric and Oceanic Sciences, Princeton University, NJ 08542**
   Email: jrussell@princeton.edu

2) **GFDL, Princeton, NJ 08542**

(In preparation for the Journal of Climate 4/29/2005)

ABSTRACT

The analyses presented here focus on the Southern Ocean as simulated in a set of global coupled climate model control experiments conducted by several international climate modeling groups. Dominated by the Antarctic Circumpolar Current (ACC), the vast Southern Ocean can influence large-scale surface climate features on various time scales. Its climatic relevance stems in part from it being the region where most of the transformation of the world ocean's water masses occurs. In climate change experiments that simulate greenhouse gas induced warming, Southern Ocean air-sea heat fluxes and 3-D circulation patterns make it a region where much of the future oceanic heat storage takes place, though the magnitude of that heat storage is one of the larger sources of uncertainty associated with the transient climate response in such model projections. Factors such as the Southern Ocean's wind forcing, heat and salt budgets are linked to the structure and transport of the ACC in ways that have not been expressed clearly in the literature. These links are explored here in a coupled model context by analyzing a sizable suite of pre-industrial control experiments associated with the forthcoming Intergovernmental Panel on Climate Change's 4th Assessment Report. A framework is developed that uses measures of coupled model simulation characteristics, primarily those related to the Southern Ocean wind forcing and water mass properties, to allow one to categorize and to some extent predict, which models do better or worse at simulating the Southern Ocean and why.

1. Introduction

During the past year, an unprecedented effort has been made by climate modeling groups to provide climate model results to the international climate research community. This effort is in support of the Intergovernmental Panel on Climate Change's Fourth Assessment report (IPCC AR4). As part of the IPCC-requested standard set of integrations, sets of control integrations, idealized forcing experiments, simulations of the past 100+ years, and multiple projections of future climate scenarios are performed. Here we analyze model output obtained from the pre-industrial control integrations of the coupled atmosphere-ocean-land surface-sea ice models participating in this exercise.

The analysis focuses on an evaluation of the Southern Ocean simulation in the pre-industrial control integrations (Picntrl in the IPCC AR4 nomenclature) of a set of atmosphere-ocean-land surface-sea ice global coupled climate models developed by several international modeling groups. In principle, a control integration's simulated climate should be steady with only variability that arises from interactions between the various components of the coupled system, since the incoming solar radiation at the top of the model atmosphere repeats exactly year after year, and the boundary conditions (the greenhouse gases, aerosol concentrations, land use, etc.) are fixed. In practice, however, all models suffer from some climate drift, which is an unforced trend away from some initial state, with the trend not being part of normally occurring variability about a constant mean state. An evaluation of this climate drift is not central to this study, however in order to compare the models, some gross analysis of the drift was required. For the purposes of this study, we found that the drifts are small enough relative to the model errors that we can just focus on those errors.

The methods used to initialize the AOGCMs (atmosphere-ocean general circulation models) are also important to the understanding of the results presented here. This is especially true as one looks at regions located further from the ocean surface. The initialization methods can vary from model to model (Stouffer and Dixon 1998), however most models use some variation of the technique documented in Stouffer et al. (2004). See PCMDI's IPCC Model Output web site (http://www-pcmdi.llnl.gov/ipcc

/model_documentation/ipcc_model_documentation.php) for more information about the individual models, including details on the initialization methods used.

The mechanisms by which winds drive the ACC have been the subject of extensive debate over the past 50 years. Attention has focused on the physics governing the mean flow. Munk and Palmen (1951) first suggested that the surface wind stress over the ACC might be balanced by form stress due to pressure gradients across topographic obstructions on the ocean floor. The momentum balances in some ocean-only numerical models of the Southern Ocean are consistent with wind stress balancing form stress (Stevens and Ivchenko, 1997; Gille, 1997), but in their simplest form do not account for the strength of the mean ACC. As an alternative to the direct forcing mechanism, Stommel (1957) pointed out that wind stress curl might drive the ACC in a fashion similar to mid-latitude Sverdrup dynamics. More recent studies based on ocean-only numerical models have suggested that in addition to wind stress and wind stress curl, buoyancy forcing may also play a role in determining ACC transport (Gnanadesikan and Hallberg, 2000; Gent et al 2001). Available data are inadequate to provide definitive explanations for the dynamical processes controlling the mean flow of the ACC, since study of the mean ACC would require not only the mean transport, but also how it would differ under alternative ocean conditions.

This study attempts to increase our understanding of what drives and determines the ACC by identifying certain relationships between the wind stress, wind stress curl, buoyancy forcing and ACC transports present in a suite of twelve coupled climate models. The analysis framework presented here provides a means to categorize and to some extent predict, the quality and nature of the different Southern Ocean simulations. It also identifies reasons why most of model-to-model differences exist. However, the analyses fall short of offering a definitive explanation of the ACC dynamics, in part due to the large variations in the model configurations

The framework presented here is only one of several ways that one might assess the quality of Southern Ocean simulations. As is typical in multi-model intercomparison studies, it is beyond the scope of this paper to examine all of the potentially relevant configuration differences that exist among the dozen coupled climate models studied here. We have chosen these analyses to explore one particular set of questions designed

to improve our understanding of how and why these twelve models' Southern Ocean simulations vary from one another and from observations, using relatively simple model diagnostics and corollary observed ocean data.

The ability of IPCC-class climate models to simulate the Southern Ocean circulation is important, since it is a part of the coupled climate system that plays an important role in the global carbon cycle and surface climate change patterns. It has been shown in earlier papers (e.g. Manabe et al. 1991, Cubasch et al. 2001) that the Southern Ocean is a region of minimum warming as greenhouse gases (GHGs) increase in the atmosphere. It is also a region where most of the oceanic heat storage is projected to occur (Sarmiento et al. 1998). The oceanic heat storage is one of the larger sources of uncertainty in future climate change projections (Cubasch et al. 2001).

In the present climate, the Southern Ocean is the region where most of the mixing of the world ocean's water masses occurs. The Southern Ocean circulation is dominated by the Antarctic Circumpolar Current that transports about 120 Sverdrups (1 Sv = 10^6 m^3 sec^{-1}) of water around Antarctica (Nowlin and Klinck, 1986). The maximum flow of the current is normally concentrated in two parallel fronts, the Subantarctic Front and the Polar Front, with the Polar Front being closer to the Antarctic continent. The Ekman drift in the surface layer is substantial, due to the strength of the westerly winds in the Southern Ocean. The northward drift in the surface waters creates a divergence south of the Polar Front, which creates vast areas of upwelling water (Peterson & Whitworth, 1989). In addition, the wind stress curl is maximized on the Polar Front, pulling water from great depth to the surface. Precipitation tends to accumulate in the surface waters during their drift northward, lowering the salinity of the water. Southern Ocean surface waters are subducted when they reach the Subantarctic Front because they are significantly colder and therefore denser than the surface waters of the subtropical gyre. These subducted Southern Ocean surface waters mix across the front forming Subantarctic Mode Water and Antarctic Intermediate Water, the building blocks of the global ocean shallow-overturning circulation.

Recent work emphasizes the importance of the region around Drake Passage and the Southeast Indian Ocean to the injection into the subtropical gyres of the two important components of the Southern Ocean intermediate and mode water circulation:

Subantarctic Mode Water (SAMW) and Antarctic Intermediate Water (AAIW) (McCartney, 1977; McCartney, 1982; Talley, 1996; Talley, 1999). The densest subduction in a subtropical gyre is of water in its poleward-eastern corner and there are only two such southeastern corners in the Southern Ocean: the southeastern Indian Ocean and the southeastern Pacific Ocean (Talley, 1996). In these two areas, the densest surface isopycnals lying north of the zero wind-stress curl are subducted to form SAMW and AAIW. Traditionally, Antarctic Intermediate Water has been identified as the salinity minimum lying at about 800 to 1000 meters depth and originating from close to the sea surface near the Antarctic Circumpolar Current and extending northward through the Atlantic, Pacific and Indian Oceans. SAMW is formed south of Tasmania as the densest subduction for the Indian Ocean (McCartney, 1977). New Antarctic Intermediate Water is linked with the surface pycnostad, SAMW, in the southeastern Pacific, where a portion becomes the Pacific AAIW and the part that flows through Drake Passage becomes Atlantic and Indian Ocean AAIW after further densification.

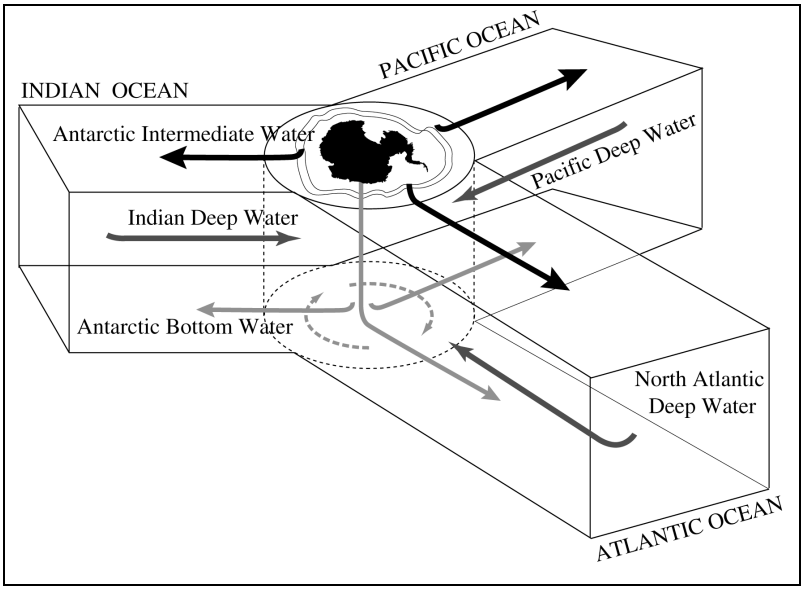

Figure 1:Cartoon of major Southern Ocean circulation features and water masses.

The Southern Ocean water mass distribution and circulation is particularly sensitive in two ways to the strength and position of the Westerly Winds. First, the position of the Westerlies relative to the topography in the poleward-eastern corners of the Pacific and Indian Oceans determines the density of the water subducted to form

SAMW and AAIW. Second, the position of the Westerlies is important because these winds produce a divergent upwelling flow along the southern boundary of the ACC. The water pulled to the surface along isopycnal surfaces by this divergence is relatively warm and salty and comes from great depth (Gordon, 1971). A component of this upwelled deep water is entrained into the Ekman layer and advected north towards the Subantarctic Front (Gordon, 1971). The formation of Antarctic Bottom Water and Circumpolar Deep Water (CDW) are also affected by the surface westerly winds through this entrainment of salt from North Atlantic Deep Water pulled into the South Atlantic through the surface divergence (Figure 1).

In addition to the effect of the high latitude heat flux from the ocean to the atmosphere, the density gradient across the ACC is determined by the relative amount of salty NADW pulled near the surface from below the sill depth of the Drake Passage. There are three obvious ways a model can get this wrong. 1) If the winds are too strong and the Southern Ocean divergence pulls too much salty water to the surface, then the water column becomes unstable and open ocean convection homogenizes the polar gyre. 2) If the model's winds are too weak or shifted too far equatorward, then the surface water divergence is weak and the upwelling of salty water is weak. 3) If a model produces too little NADW or the NADW produced is too warm or too fresh, the density gradient across the current cannot be maintained and the ACC transport weakens. We will present evidence that the ability of the ocean model to export salty North Atlantic Deep Water into the Southern Ocean is the most significant internal ocean contribution to the variability between the twelve IPCC AR4 models studied here.

Our analysis will focus on the stability of the Southern Ocean (roughly the density stratification) and the ways in which this is affected by the strength of the surface westerlies, the position of the surface westerlies, and the volume, heat and salt transport of NADW exported into the Southern Ocean. The wind forcing and the salinity budgets of the Southern Ocean are intimately linked in ways that have not been clearly expressed in the literature. The existence of a suite of model runs conducted for the IPCC AR4 has given us the chance to demonstrate this link and to use the strengths of various parameters to predict which models do better or worse and why.

2. Antarctic Circumpolar Current Transport

Particularly at high latitudes where the ocean is weakly stratified, currents tend to be vertically coherent (or barotropic) due to the earth's rotation. These currents steer around major topographic features, like ridges and seamounts, which they cannot pass through. Since ocean surface currents align in roughly the same direction as deep ocean currents, they tend to follow contours of constant depth; thereby detouring around the bumps and troughs in the seafloor (Schulman, 1975). Contours of sea surface height (SSH) and barotropic streamfunctions (Fig 2) will thus tend to reflect the bottom topography (Fig 3).

Figure 2a shows the observed annually averaged sea-surface height from the TOPEX data. We present this as a proxy for the barotropic streamfunction since the free surface is directly related to the pressure gradient and therefore the barotropic transport. In the Southern Hemisphere, low pressure (blue) drives a clockwise flow around the Antarctic continent. The barotropic streamfunction is presented for each of the IPCC models for which it is available, with the blue shading indicating a clockwise flow and the red shading counter-clockwise. For those models that did not report a barotropic streamfunction (GISS-AOM (k) and GISS-EH (l)) we present the simulated sea-surface height.

All of the models correctly simulate the eastward flow through the Drake Passage (except for the GISS-EH model which has a strong westward flow at the bottom). The GFDL-CM2.0(b), GFDL-CM2.1(c), MIROC3.2(hires)(g) and MRI-CGCM2.3.2a(j) are all within 20% of the observed transport of 115 Sv (see Table 1). Several of the models have much too high flow (well over 200 Sv); these are the UKMO-HadCM3(d), GISS-AOM(k), GISS-ER(m), and CSIRO-Mk3.0(h) runs. The CNRM-CM3(e) and IAP-FGOALS1.0g(i) experiments underestimate the net transport.

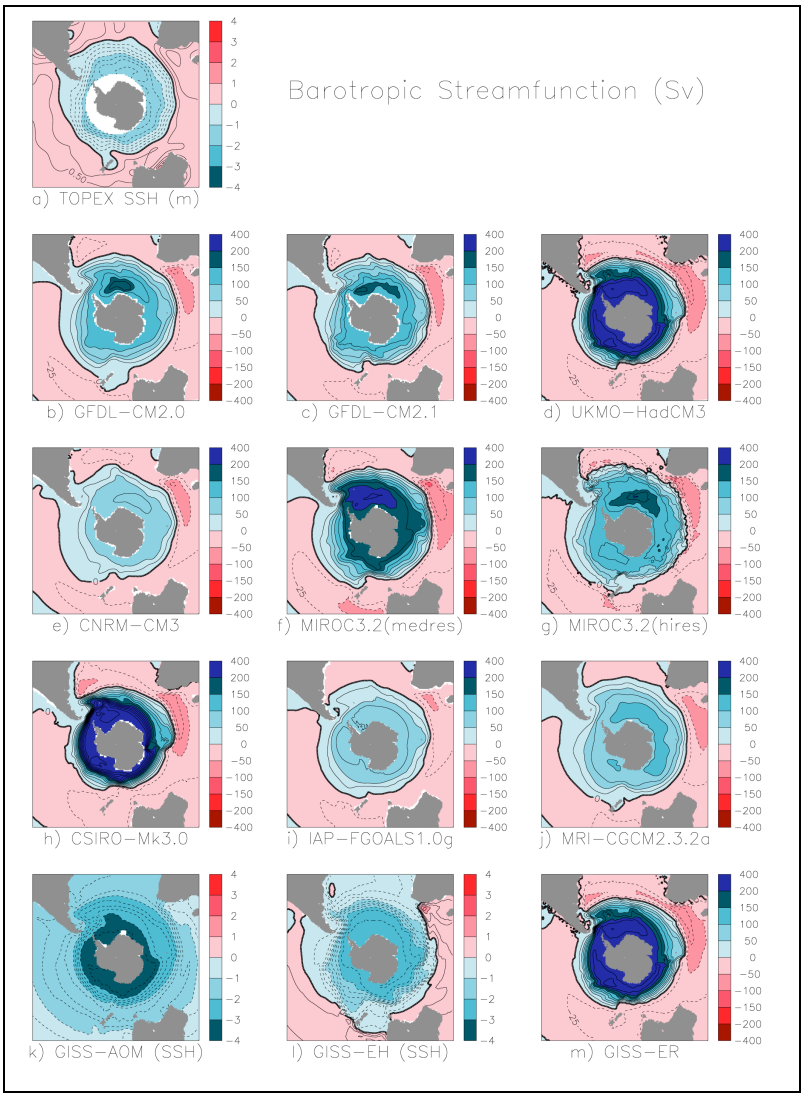

Figure 2: Free-surface elevation (in m) and barotropic streamfunction (in Sv) from the observations and the IPCC ocean simulations. All panels are the barotropic streamfunction, except for panels a), k) and l). The streamfunctions for the GISS-AOM, and the GISS-EH simulations are currently unavailable.

The oceanic bathymetry around Antarctica from the ETOPO 40' observational dataset is presented in Figure 3a. The main features that intersect the ACC (from the top and moving clockwise) are the Mid-Atlantic Ridge, the Kerguelen Plateau, Tasmania and the Campbell Plateau, the East Pacific Rise, South America and the Scotia Arc. Each of these influences the path of the circumpolar current. In ocean models with limited grid resolution, however, the imposed bathymetry is almost as much art as it science: attempts can be made to "tune" topographic features to correct for known shortcomings in a

model's simulation and to more accurately reflect the influence of the ocean topography on the mean flow at the model's resolution.

In the models from GFDL (b, c), UKMO (d), MIROC (f,g), IAP (i), MRI (j), and GISS (k,l,m) the errors (i.e., differences between the observed and modeled bathymetry) look random, limited by grid resolution. However, all models exaggerate the underwater mountain north of New Zealand.

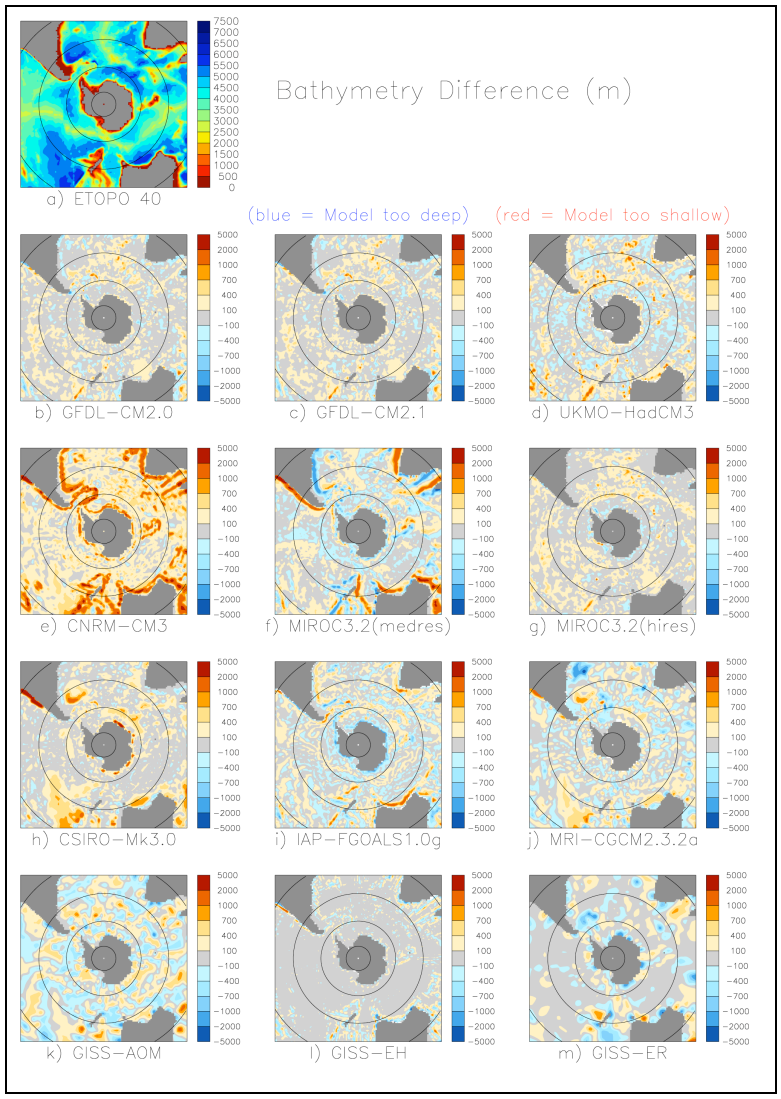

Figure 3: Bathymetry and the differences from observed for the IPCC models used in this study. Latitude lines at 80S, 60S, 40S and 20S are indicated. All units in meters.

In CSIRO-Mk3.0 (h), the Southern Ocean bathymetry values are somewhat too high with relatively large positive errors in the South Atlantic and over a large region east

of New Zealand. In the CNRM-CM3 (e), the values are too high almost everywhere and the Scotia Arc is severely exaggerated. This error many be exaggerated by the interpolation of the model grid onto the grid used for the models in the PCMDI database. However, it appears to us that some of these problems are real, that is, they are adversely affecting the flow in CNRM-CM3. As will be shown later, these topographic differences lead to a weaker ACC, due to increased bottom drag and a subdued ACC retroflection into the Malvinas Current associated with the barrier of the Arc.

The reasons for the non-random errors in some models' topographic fields are unclear. To fully understand these differences, one would have to consult in detail with each modeling group to determine the exact reasons for the relatively poor representation of the observed ocean topography.

As expected, the strength of the ACC scales with both the strength of the maximum wind stress (the barotropic component, Figure 4a), and the mean density gradient across the current (Figure 4b). The CSIRO-Mk3.0 simulation (red crosses) has the strongest wind stress (~30% greater than the NCEP long-term mean), the largest density gradient and an unrealistically large transport of over 330 Sv. The GISS-EH model (yellow crosses) on the other hand has the lowest wind stress (~40% less than NCEP) and an unrealistic net westward flow through the Drake Passage. The complex water mass structure in the Southern Ocean leads to differing effects of the thermal (Figure 4c) and haline (Figure 4d) gradients on the strength of the ACC. The models show distinct correlations between the temperature differences and salinity differences between 65S and 45S and the modeled ACC transport. We will present evidence that the ability of the ocean model component of a global coupled climate model to export salty North Atlantic Deep Water into the Southern Ocean is the most significant internal ocean contribution to the inter-model ACC simulation differences.

Several of the models are clustered close to the observed values (black circles) in all four panels of Fig. 4: GFDL-CM2.1 (blue circles), GFDL-CM2.0 (red circles) and MIROC3.2(hires) (cyan circles) are closest, and MRI-CGCM2.3.2a (magenta circles) and IAP-FGOALS1.0g (green crosses) are next, especially in Fig 4b. The UKMO-HadCM3 simulation (blue crosses) has reasonable winds, but also has an excessive salinity gradient

and therefore an overly vigorous ACC. The three GISS models (yellow symbols) are outliers in one or more of the figures and do not seem to fit the general linear trends.

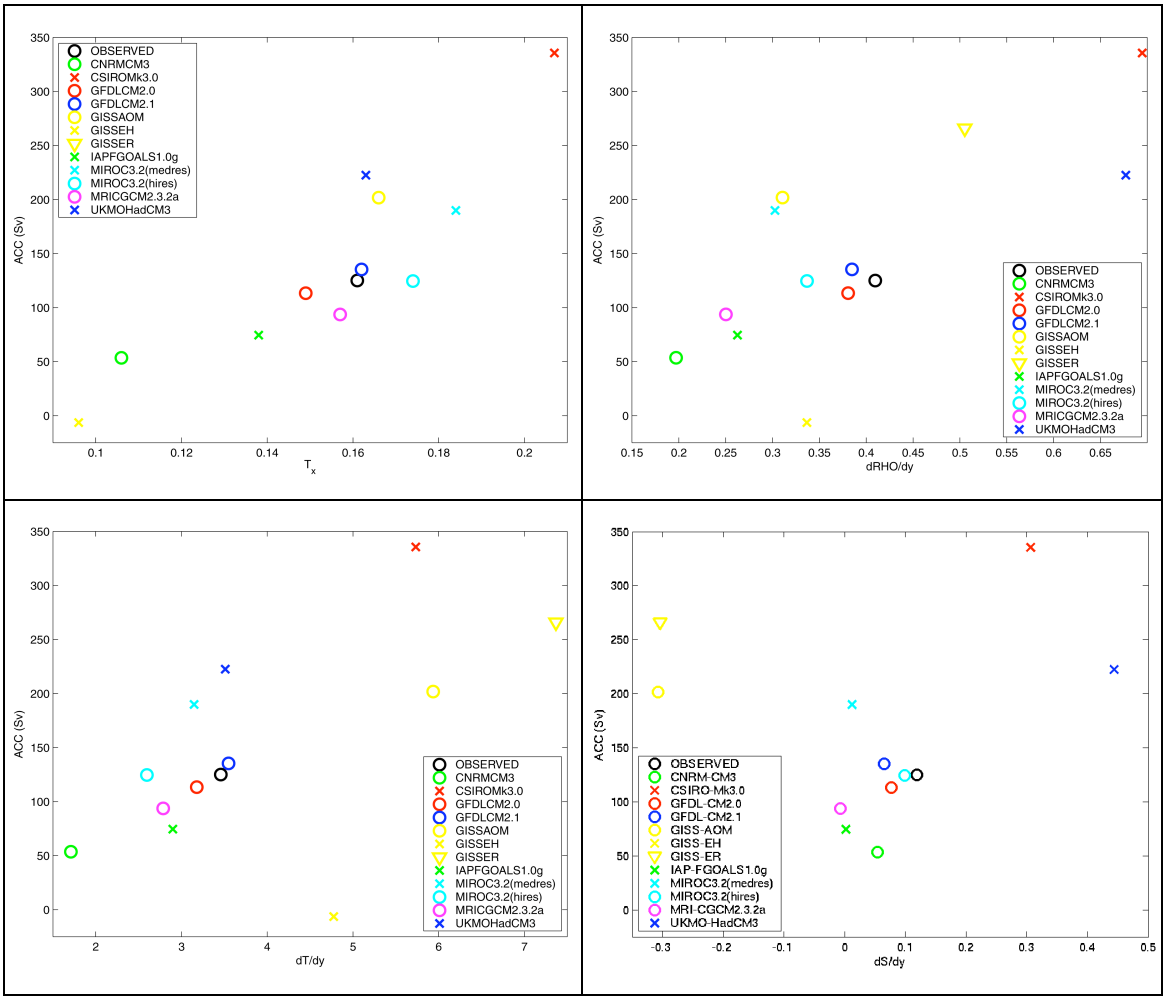

Figure 4: The maximum wind stress between 70S and 30S (N/m^2) (a) and the zonally and depth averaged (0-2500m) difference in density (b), temperature (c), and salinity (d) between 65S and 45S in each of the IPCC models and the observations, plotted against the ACC transport at Drake Passage (69°W).

In Figure 4, the three GISS models (yellow symbols) appear as outliers, with little or no salinity gradient across the ACC and an exaggerated thermal gradient. Similarly, in other figures, one or more of the GISS model do not seem to fit the general linear trends. While not fully understood, in some key ways the GISS models' representations of the Southern Ocean region seem to fall outside the range that can be readily explained using the analysis framework adopted in this study.

Various parameters relating to the strength of the ACC that are discussed in this analysis are presented in Table 1. As was seen in Fig. 2 and Fig. 4, the ACC scales with both the maximum wind stress and the salinity gradient, which is represented here by the salt export into the Southern Ocean in the NADW layers. This will be discussed in much more detail in Section 4. Also influencing the ACC transport are the position of the peak Surface Westerly Winds (i.e. the location of the zero wind stress curl) and the strength of the wind stress in the Drake Passage latitudes. The models that capture the transport most accurately are the GFDL runs and the MIROC (hires) run. The MRI simulation is a bit on the low side and MIROC (medres) is on the high side. Several of the models have excess flow through the Drake Passage: the UKMO, CSIRO, GISS-AOM and GISS-ER runs each have over 200 Sv (roughly double the observations). CNRM and IAP on the other hand have significantly weaker transport than observed.

Model	ACC (Sv)	NAOT (Sv)	NADW Salt @ 30S (10^6kg)	Max t_x (N/m^2)	Latitude of Max t_x	t_x at 60S (N/m^2)
OBSERVED	115±10	15-20		0.161	52.4	0.106
GFDL-CM2.0	101.5	16.7	657	0.149	47.0	0.047
GFDL-CM2.1	135.5	24.0	818	0.162	52.0	0.105
UKMO-HadCM3	222.5	22.1	490	0.163	51.3	0.087
CNRM-CM3	53.6	25.6	342	0.106	46.0	0.002
MIROC3.2 (medres)	189.9	21.8	506	0.184	46.0	0.035
MIROC3.2 (hires)	124.6	20.0	470	0.174	46.5	0.074
CSIRO-Mk3.0	335.6	19.7	420	0.207	51.3	0.098
IAP-FGOALS1.0g	74.6	14.2	287	0.138	48.8	0.047
MRI-CGCM2.3.2a	93.7	20.8	162	0.157	48.8	0.064
GISS-AOM	201.7	42.9	23	0.166	43.5	-0.008
GISS-EH	-6.4	26.7	50	0.096	46.0	0.049
GISS-ER	265.8	32.1	80	0.107	46.0	0.060

Table 1: Various Parameters related to the strength of the ACC.

3. Surface forcing of the Southern Ocean

The zonally averaged zonal wind stress and zonal wind stress curl are presented in Figure 5. The observations (from NCEP, black, circles) have the southernmost peak and the GFDL-CM2.1 simulation (blue, circles) is the best representation in terms of position and strength. The peak wind stress in UKMO-HadCM3 (red, circles) and the CSIRO-Mk3.0 (red, crosses) are south of 50S, but much too far equatorward in each of the other models. The CSIRO simulation is 25% too strong, and the CNRM-CM3 (blue, dashed), GISS-EH (green, dashed), and GISS-ER (cyan, dashed) simulations are 30% too weak.

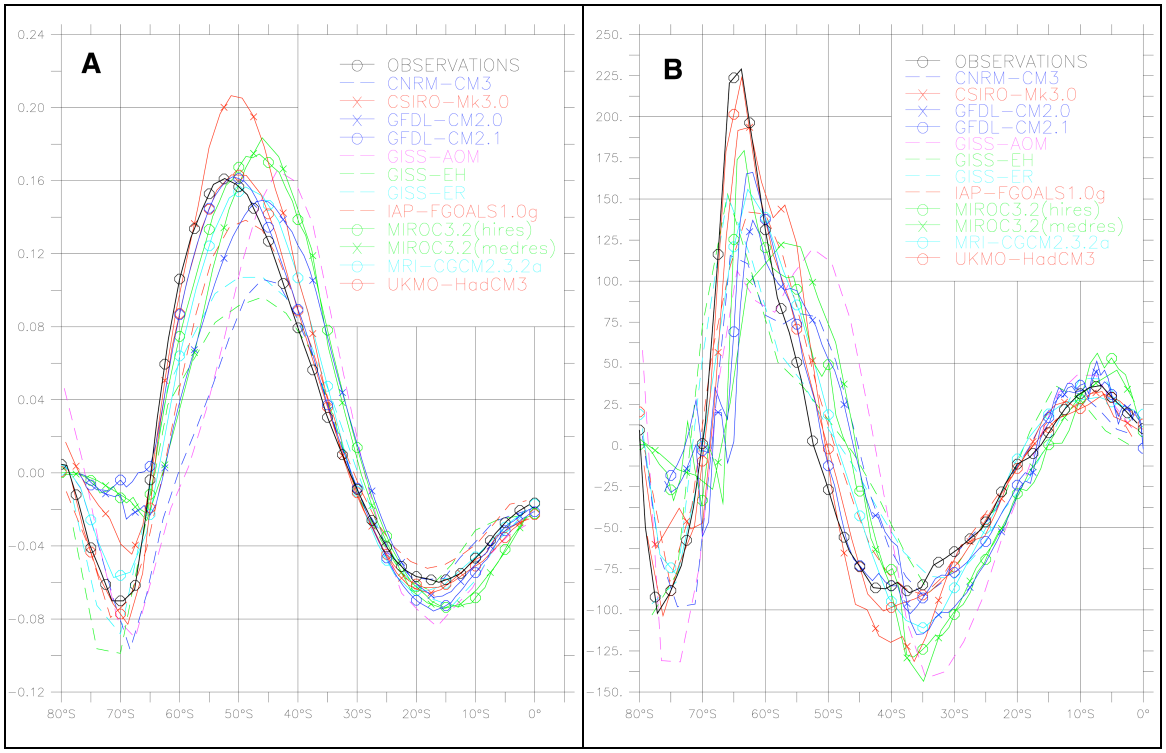

Figure 5: A) Zonally-averaged wind stress (N/m^2) and B) zonally-averaged zonal wind stress curl (10^9 N/m^3). Observed (black, circles), GFDL-CM2.1 (blue, circles), GFDL-CM2.0 (blue, crosses), CNRM-CM3 (blue, dashed), GISS-AOM (magenta, dashed), GISS-EH (green, dashed), GISS-ER (cyan, dashed), UKMO-HadCM3 (red, circles), CSIRO-Mk3.0 (red, crosses), MIROC3.2 (hires) (green, circles), MIROC3.2 (medres) (green, crosses), IAP-FGOALS1.0g (red, dashed), MRI-CGCM2.3.2a (cyan, circles).

The position and strength of the maximum wind stress curl is tied to the upwelling along the southern edge of the ACC. The UKMO-HadCM3 (red, circles) is clearly the

best. The CSIRO-Mk3.0 (red, crosses), GFDL-CM2.1 (blue, circles) and GISS-AOM (magenta, dashed) are reasonably close, and the others are both too weak and too far equatorward.

Figure 6 shows the zonally averaged heat and fresh water fluxes in the Southern Hemisphere. The models are all in close agreement with each other. Compared to the observational estimates (da Silva et al., 1994), all of the other models underestimate the heat loss at 30S and overestimate the heat loss between 50S and 70S. The IAP-FGOALS1.0g has an overly positive E-P at 60S, and the MIROC3.2(hires) has several spiky positive features.

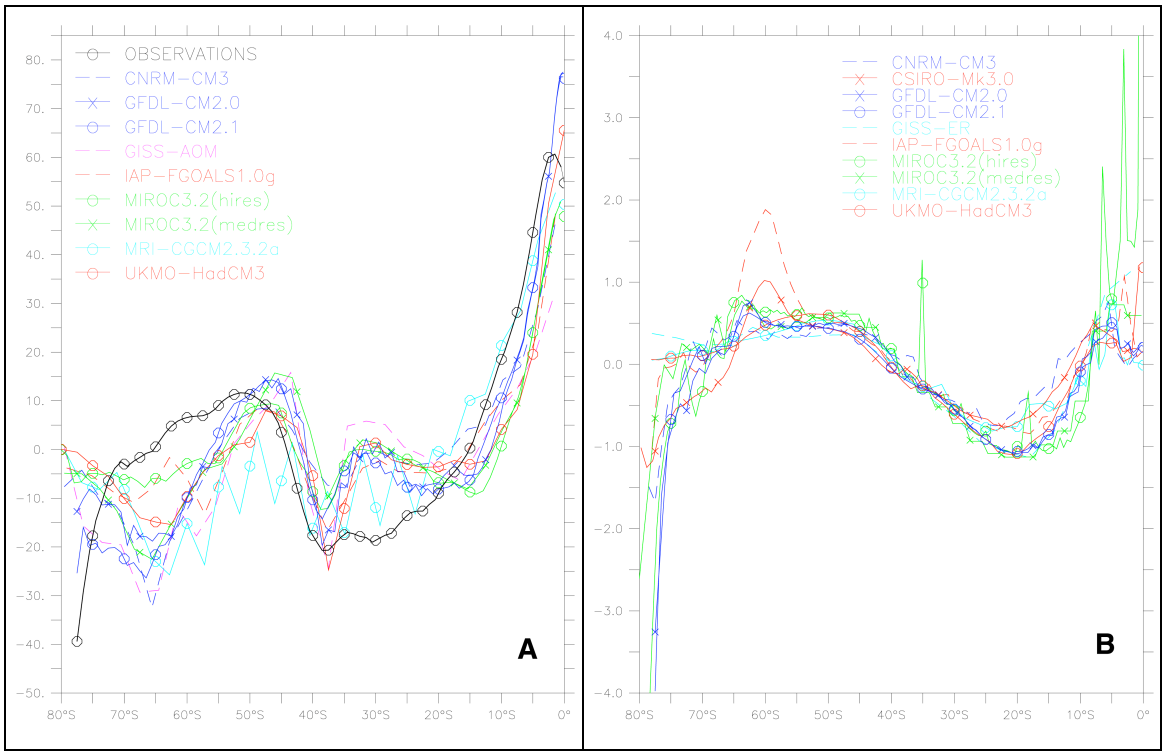

Figure 6: A) Zonally-averaged surface heat flux in W/m^2; B) zonally-averaged fresh water flux in m/yr. The heat flux is the sum of the latent heat, sensible heat, and downward and upward longwave and shortwave heating at the surface. Observed (black, circles), GFDL-CM2.1 (blue, circles), GFDL-CM2.0 (blue, crosses), CNRM-CM3 (blue, dashed), GISS-AOM (magenta, dashed), GISS-ER (cyan, dashed), UKMO-HadCM3 (red, circles), CSIRO-Mk3.0 (red, crosses), MIROC3.2 (hires) (green, circles), MIROC3.2 (medres) (green, crosses), IAP-FGOALS1.0g (red, dashed), MRI-CGCM2.3.2a (cyan, circles).

The zonally- and annually-averaged sea ice cover for each of the models is shown in Figure 7. The CSIRO-Mk3.0 (red, crosses) and MRI-CGCM2.3.2a (cyan, circles) are

closest to the observations (from Taylor et al, 2000; black, circles). Most of the models underestimate the sea-ice cover. The IAP-FGOALS1.0g model (red, dashed) has nearly permanent, total ice cover out to 60S and is also the coldest model south of 60S (see Figure 8).

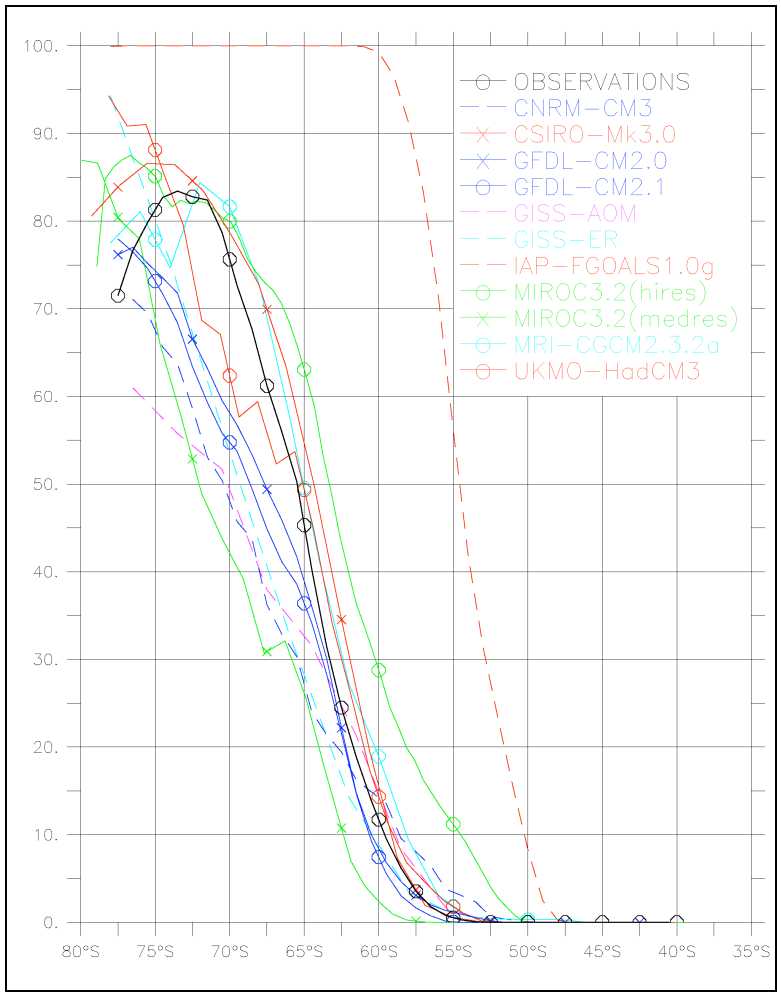

Figure 7: Zonally averaged sea ice cover as a percentage. The GISS-EH simulation is omitted as this data is not currently available. Observed (black, circles), GFDL-CM2.1 (blue, circles), GFDL-CM2.0 (blue, crosses), CNRM-CM3 (blue, dashed), GISS-AOM (magenta, dashed), GISS-ER (cyan, dashed), UKMO-HadCM3 (red, circles), CSIRO-Mk3.0 (red, crosses), MIROC3.2 (hires) (green, circles), MIROC3.2 (medres) (green, crosses), IAP-FGOALS1.0g (red, dashed), MRI-CGCM2.3.2a (cyan, circles).

The zonally averaged temperature and salinity in the uppermost 100m of the water column for each model are presented in Figure 8. The model simulations capture

the surface temperature distribution reasonably well. The GISS-EH (green, dashed) simulation is much too warm at high-latitudes. The GISS-AOM (magenta, dashed), GISS-ER (cyan, dashed) and UKMO-HadCM3 (red, circles) simulations are several degrees too warm at the equator, while the GFDL-CM2.0 (blue, crosses), CSIRO-Mk3.0 (red, crosses), and MRI-CGCM2.3.2a (cyan, circles) are several degrees too cold. The simulations show much more variability in their representation of the surface salinity (Figure 9b). Across the ACC (between 60S and 50S), most are within a few tenths of a psu, but the UKMO-HadCM3 (red, circles) is much too fresh, and the GISS-EH (green, dashed) is much too salty. Most of the models underestimate the surface salinity at 35S; this is likely due to errors in the injection of sub-tropical salt by excessively weak East Australian and Agulhas currents.

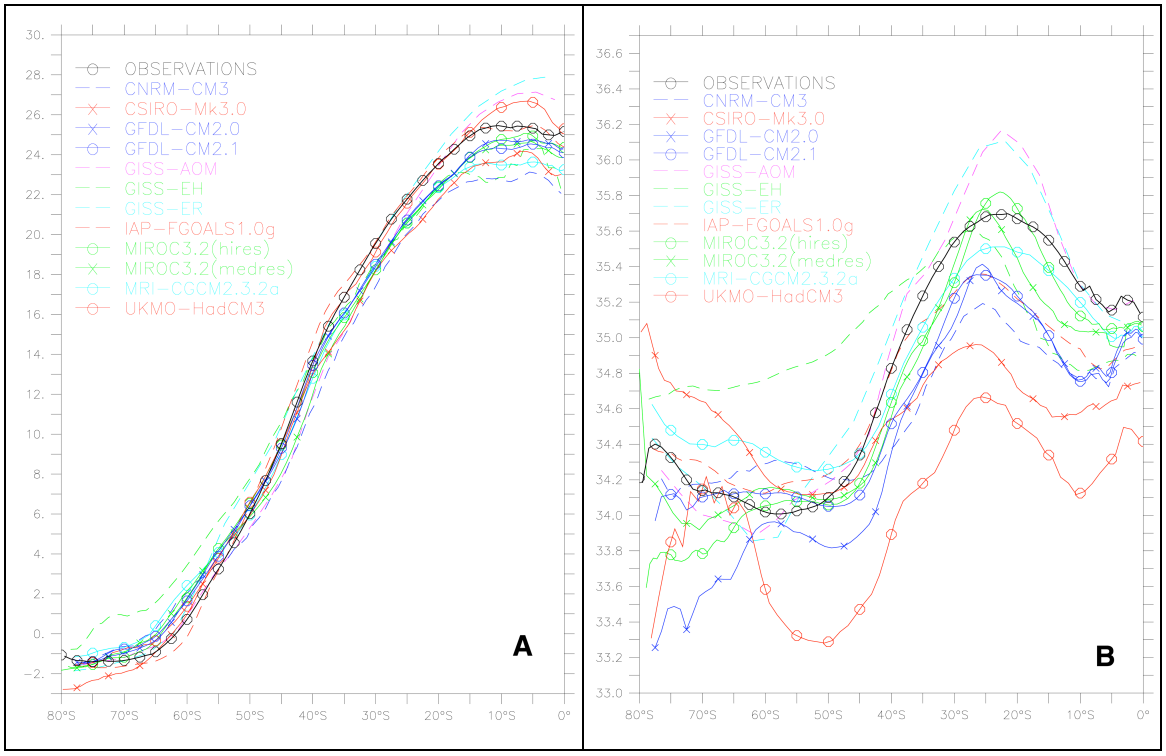

Figure 8: A) Zonally-averaged temperature (°C, 0-100m average) and B) salinity (psu, 0-100m average). Observed (black, circles), GFDL-CM2.1 (blue, circles), GFDL-CM2.0 (blue, crosses), CNRM-CM3 (blue, dashed), GISS-AOM (magenta, dashed), GISS-EH (green, dashed), GISS-ER (cyan, dashed), UKMO-HadCM3 (red, circles), CSIRO-Mk3.0 (red, crosses), MIROC3.2 (hires) (green, circles), MIROC3.2 (medres) (green, crosses), IAP-FGOALS1.0g (red, dashed), MRI-CGCM2.3.2a (cyan, circles).

Figure 9 shows the average salinity difference in the top 100m (model – observations) for the reported IPCC ocean models. As was seen in Figure 8b, GISS-EH(l) is much too salty, and UKMO-HadCM3(d) is much too fresh. Most of the errors are zonally symmetric and seem to be associated with deviations in the locations of the strong salinity gradients, especially east of Argentina and south and east of South Africa.

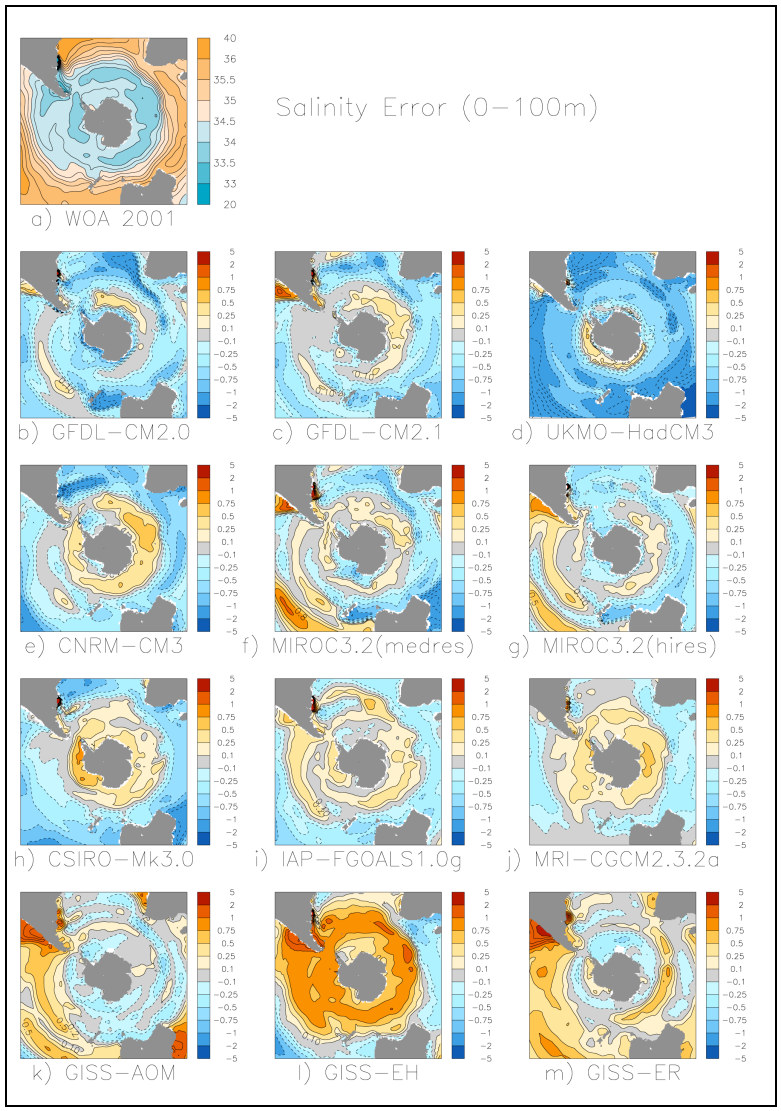

Figure 9: Salinity differences (psu) from the observations (a) in the uppermost 100m from 12 of the IPCC ocean models. Positive values indicate that the model is more saline than observed.

The salinity anomalies are also closely linked to the wind curl anomalies seen in Figure 5b. As was previously noted, all of the models have the peak winds (and thus, the zero

wind-stress curl) too far northward by 1 to 10° of latitude. This alters the divergence at the southern edge of the ACC and thus the upwelling.

Models with too high salinity adjacent to Antarctica tend to have too great communication between the surface and the deep ocean. The high salinity near the Antarctic coast is both a cause and an effect. The high surface salinity tends to destabilize the water column increasing the vertical mixing. The increased mixing brings more salt from depth to the surface. Models, on the other hand, with small or patchy salinity errors south of 60S are more stably stratified. One counter-example, however, is the CNRM-CM3 simulation; although the surface salinities are too high most of the way around the continent, the deep salinities are even higher (see Fig. 12), leading to a too stable profile. The MIROC3.2 (medres and hires) runs are similar to each other. These have alternating bands of high and low salinity spiraling out from the continent. The simulations with weaker ACC transport (CNRM-CM3, IAP-FGOALS1.0g and MRI-CGCM2.3.2a) all have too low surface salinities on the equatorward edge of the ACC.

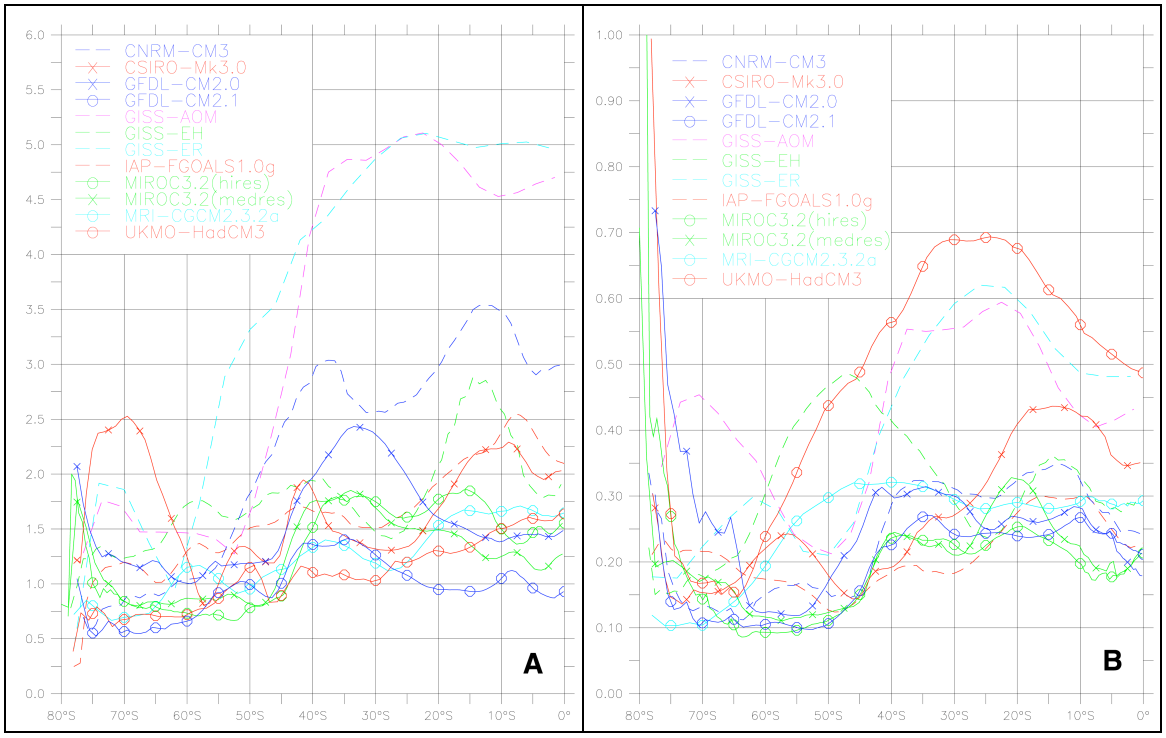

Figure 10: A) Zonally-averaged RMS errors in temperature (°C, surface -1500m) and B) salinity (psu, surface -1500m). GFDL-CM2.1 (blue, circles), GFDL-CM2.0 (blue, crosses), CNRM-CM3 (blue, dashed), GISS-AOM (magenta, dashed), GISS-EH (green, dashed), GISS-ER (cyan, dashed), UKMO-HadCM3 (red, circles), CSIRO-Mk3.0 (red, crosses), MIROC3.2 (hires) (green, circles), MIROC3.2

(medres) (green, crosses), IAP-FGOALS1.0g (red, dashed), MRI-CGCM2.3.2a (cyan, circles).

The zonally averaged root-mean squared (rms) temperature and salinity errors averaged of the top 1500 meters of the water column for each model are shown in Figure 10. The GFDL-CM2.1 simulation (blue, circles) is the most successful in the Southern Hemisphere with both tracers, although the IAP-FGOALS1.0g (red, dashed) appears to have lower salinity rms errors and larger temperature errors when compared to GFDL_CM2.1. Most of the models simulate the temperature more accurately south of 60S than they do north of that latitude. Several of the models, most notably the two MIROC submissions (green, circles and crosses) and the UKMO experiment (red, circles), have large salinity errors adjacent to the Antarctic continent. These three models all overestimate the annual percent coverage of sea-ice south of 75S. The GISS-AOM and GISS-ER models do the least well north of 40S: both are too warm (~5C) and too salty (> 0.5psu). Note that the models with large salinity deviations north of 40S (UKMO, GISS-AOM, and GISS-ER) all have excessive ACC transport.

4. Water Mass Simulations

The global overturning streamfunctions for each model are presented in Figure 11. The structure is relatively consistent in all of the models except for GISS-EH (k), and the two MIROC models (e,f). Similarities between the simulations include a prominent, clockwise overturning in the northern hemisphere, a strong Deacon Cell (the clockwise overturning at 50S, and a counter-clockwise cell in the lower ocean. There are wide differences in terms of magnitude however.

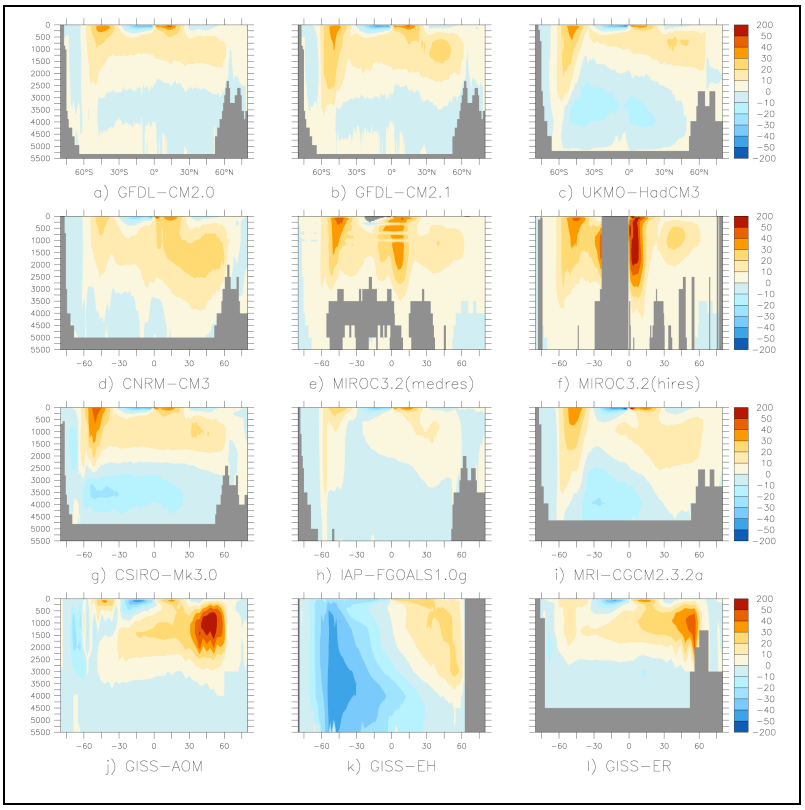

Figure 11: Global overturning streamfunction. Positive values indicate a clockwise circulation. Units are in Sv (10^6 m^3/s). The GFDL and UKMO overturnings have been calculated from the meridional velocity: the other data are that reported to the PCMDI.

Estimates of North Atlantic Deep Water formation are on the order of 15-20 Sv (Schmitz et al., 1996) with the main southward flow between 2000 and 3500m. By these criteria, the best representations are the GFDL-CM2.0(a), GFDL-CM2.1(b), CSIRO-Mk3.0(g), and UKMO-HadCM3(c) although the UKMO simulation is considerably shallower. The GISS-AOM(j) and the GISS-ER(l) simulations are much too strong (more

than 40 SV), and the IAP-FGOALS1.0g(h) is much too weak. The MRI-CGCM2.3.2a(i) simulation is slightly too weak (less than 15 SV), although the structure is roughly correct. The GISS-EH(k) simulation has two hemispheric counter-rotating cells extending from the surface to the bottom. This may be due to interpolation problems in going from the model's native isopycnal coordinates to the Z-level coordinates used to archive the model output.

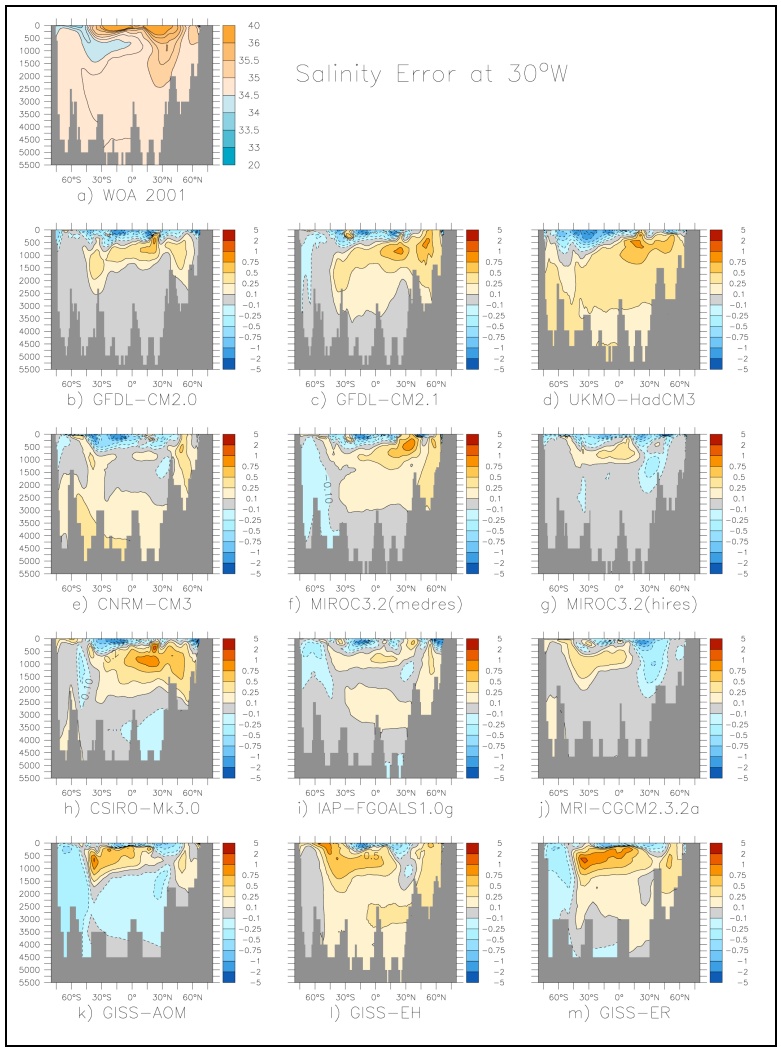

Figure 12: Salinity differences from the observations (a) along 30°W from 12 of the IPCC ocean models. Positive values indicate the model is more saline than observed.

The salinity structure along 30W in the Atlantic shows most of the major oceanic water masses. Relatively high salinity (> 34.75) North Atlantic Deep Water is observed to be filling the basin between 1500 and 4000 meters (Figure 12). Also seen are the intermediate salinity bottom waters flowing northward, the low salinity (< 34.5) Antarctic

Intermediate Water subducting at 45S and moving northward at ~800 meters, along with the salty subtropical gyres and the Mediterranean outflow (at 30N at 1000m). Separation of the models into the overstable, understable and "about right" classes is easiest here. GISS-EH, MRI and CSIRO all have positive salinity anomalies at the surface overlying negative anomalies at depth, and all three models are understable (too unstable). The other two GISS models (AOM and ER) along with the IAP, UKMO and MIROC (medres) runs, also show clear indications of too light water above and too dense water below, clear signs of overstability. Only the two GFDL simulations and the MIROC (hires) seem to occupy the middle ground.

We now present a more detailed analysis of the circulation in the South Atlantic at 32S. Talley (2003) decomposed the density structure into 6 classes, representing the Ekman transport, the upper thermocline between the surface and s_0=26.2, the lower thermocline between 26.2 and 26.9, the AAIW layer between 26.9 and 27.4, the NADW layer between s_0=27.4 and s_4=45.86, and AABW between 45.86 and the bottom, and we have done the same type of analysis here. We have subdivided each layer into 4 sub-layers to perform a more detailed analysis. The only technical issue was in dividing the NADW layer into sub-classes that do not overlap. We determined that in none of the model simulations was the s_0=27.6 contour below the s_4=45.86 contour so Talley's NADW was divided into layers between 27.4 and 27.45, 27.45 and 27.5, 27.5 and 27.6 and 27.6 and 45.86.

Talley determined that the southward flow of 17.8 Sv of NADW is balanced by northward flows in the other layers (Figure 13a). The GFDL-CM2.1 (c), GFDL-CM2.0 (b), and MIROC3.2(medres) (f) simulations are clearly the most realistic, although there are sizeable errors in many density ranges. The CSIRO-Mk3.0 run (h) is reasonably close to the observations in that each layer has its transports in the right direction. The UKMO-HadCM3 (d), IAP-FGOALS1.0g (i), and MIROC3.2(hires) (g) experiments are weak, but the flows seem to be slightly offset from their observed density class. The other 4 models, CNRM-CM3 (e), GISS-AOM (k), GISS-ER (m), and MRI-CGCM2.3.2a (j) all have extremely weak integrated flows implying that not much density change is exported to the Southern Ocean in these models as part of the North Atlantic overturning. The GISS-EH (l) model has reasonably strong transports, but as was seen in the global overturning

streamfunction (Fig 11l), there is southward flow in the upper layers and northward flow at the bottom.

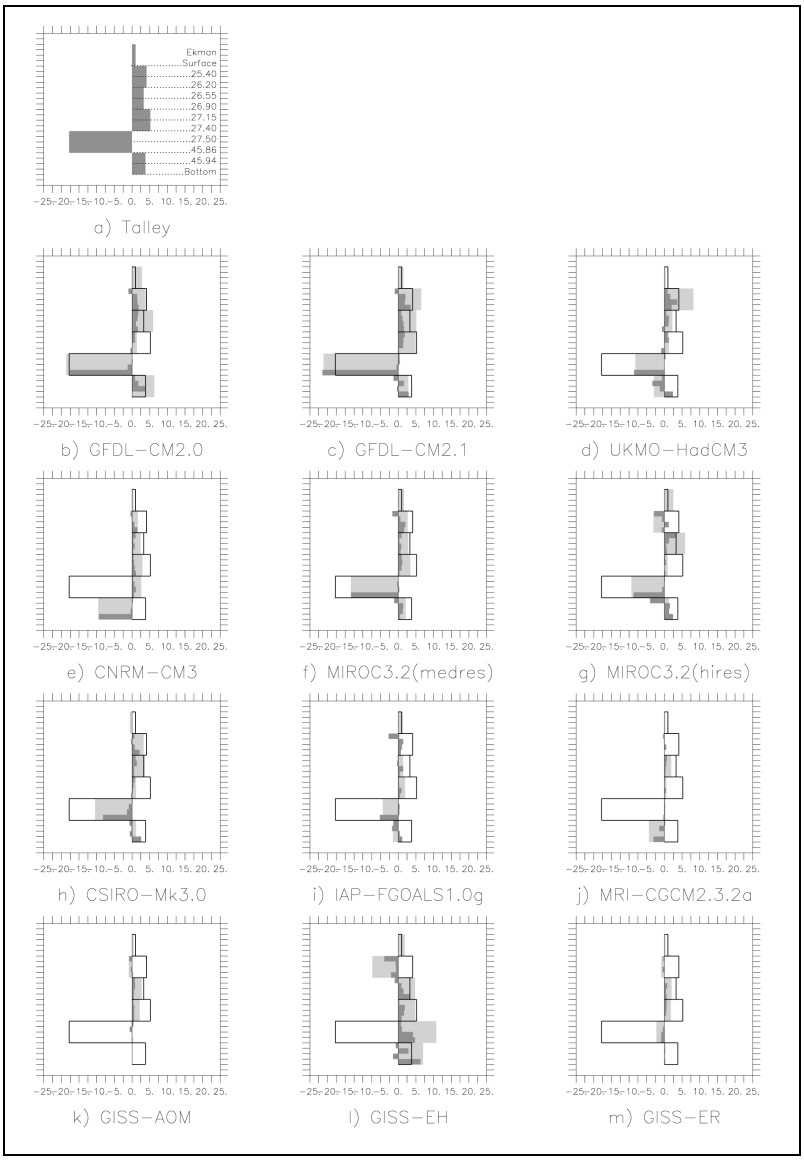

Figure 13: Inverse transport calculations across 32°S in the Atlantic (between 60°W and 20°E) based on the layer definitions in Talley (2003). The pale gray bars are the integrated totals for each layer and can be compared to the black lines, which are the observed values from Talley (2003). The dark gray bars are approximately equal subdivisions of each layer. The Ekman layer transport is calculated from the wind stress and is subtracted from the uppermost layer transport. Positive values are northward transport, and the units are in Sv (10^6 m^3/s).

The meridional heat transports from each of the models is presented in Figure 14. All simulations have roughly the same shape as the observations (from Trenberth and Caron, 2001, black, circles) with northern hemisphere maxima in the sub-tropics

decreasing to the pole, and southern hemisphere maxima in the sub-tropics and at ~50S. All of the models (except for the GISS-EH, green, dashed) underestimate the southward heat transport in the Southern Hemisphere between the equator and 30S and most underestimate it south of there. The MIROC models (green, circles and crosses) and the IAP-FGOALS1.0g (red, dashed) underestimate the northern hemisphere maximum. The common underestimation of the southward heat transport at 20S seems related to problems in simulating the East Australian and the Agulhas currents. The CNRM-CM3 experiment (blue, dashed) has almost no southward heat transport at 15S and nearly double the observed at 40S. These errors lead to the weak barotropic streamfunction seen in Fig 2e. The Southern Ocean in the CNRM-CM3 experiment is too warm (not shown) due to this excessive heat transport and the density gradient is therefore greatly reduced, leading to a relatively weak ACC.

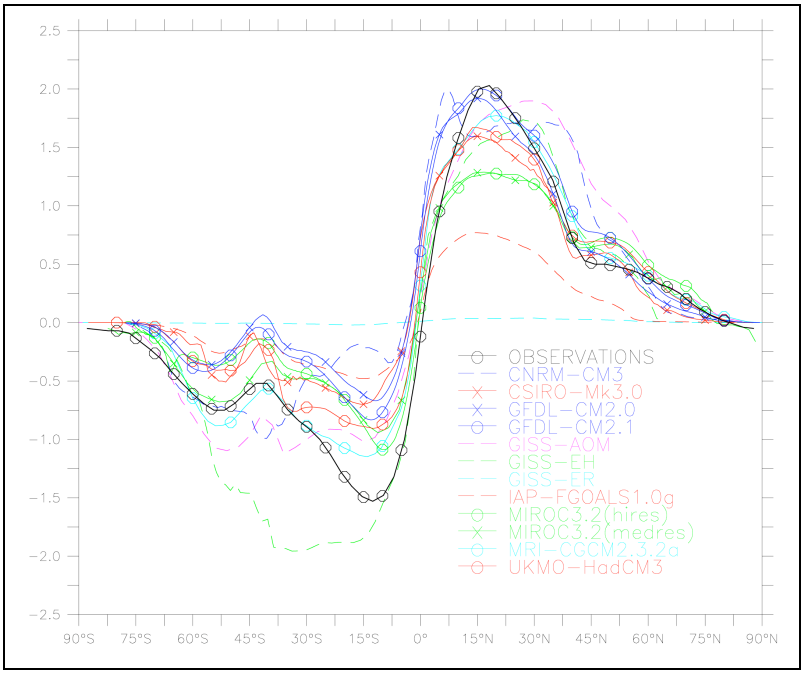

Figure 14: Zonally integrated meridional heat transport. Observed (black, circles), GFDL-CM2.1 (blue, circles), GFDL-CM2.0 (blue, crosses), CNRM-CM3 (blue, dashed), GISS-AOM (magenta, dashed), GISS-EH (green, dashed), GISS-ER (cyan, dashed), UKMO-HadCM3 (red, circles), CSIRO-Mk3.0 (red, crosses), MIROC3.2 (hires) (green, circles), MIROC3.2 (medres) (green, crosses), IAP-FGOALS1.0g (red, dashed), MRI-CGCM2.3.2a (cyan, circles). Units in PW (PW = 10^{15} W).

The primary process identified here by which the oceanic simulation in a coupled model can affect the ACC is the salinity export of NADW into the Southern Ocean that

upwells on the Antarctic side of the current. Table 2 presents several indicators relating to the formation and export of NADW in each of the IPCC models discussed in this study. We find that the models with the best overall ACC transports and Southern Ocean water masses are those in which the outflow of NADW across 30S is both strong (> 14Sv) and saline (> 34.85psu), like the GFDL runs and the MIROC(medres) run. Several models have strong overturning in the North Atlantic that is not carried into the Southern Ocean (CNRM, MRI and the GISS simulations). NADW is warmer than recycled Circumpolar Deep Water (CDW); models with a strong southward flow combined with a weak heat transport have too much bottom water in the NADW outflow layers (the CSIRO and MIROC(hires) models). While the UKMO simulation has reasonable salt export, heat export and wind strength, the ACC is overly strong due to the major negative salinity anomalies on the north side of the current seen in Fig 9d.

Model	Maximum NAOT (Sv)	NADW @30S (Sv)	Salinity of NADW	NADW Salt Export (10^6kg)	NADW Heat Export (PWC)
OBSERVED	15-20	15-20			
GFDL-CM2.0	16.7	18.8	34.92	657	-0.33
GFDL-CM2.1	24.0	23.3	34.97	818	-0.41
UKMO-HadCM3	22.1	13.9	35.01	490	-0.26
CNRM-CM3	25.6	9.8	34.93	342	-0.09
MIROC3.2 (medres)	21.8	14.4	34.88	506	-0.27
MIROC3.2 (hires)	20.0	13.5	34.73	470	-0.15
CSIRO-Mk3.0	19.7	12.0	34.84	420	-0.23
IAP-FGOALS1.0g	14.2	8.2	34.84	287	-0.09
MRI-CGCM2.3.2a	20.8	4.7	34.83	162	-0.04
GISS-AOM	42.9	0.7	34.72	23	-0.01
GISS-EH	26.7	1.4	34.89	50	-0.01
GISS-ER	32.1	2.3	34.96	80	-0.06

Table 2: Various Parameters related to the strength of NADW Formation and Export.

5. Discussion

Assessing the performance of coupled models in the context of the ACC transport is complex, encompassing performance issues from the atmosphere, ice and ocean components of the models. Returning to the relationships between the ACC transport and the wind stress, temperature gradient and salinity gradient in Figure 4, we find that the most important gauges for assessing the likely Southern Ocean simulation performance, in descending order of importance, are 1) the strength of the westerly wind over the Drake Passage latitude band, 2) the air-sea heat flux gradient over the same latitude band (although this quantity is relatively well simulated by the models presented here and therefore introduces little of the observed intermodel differences presented here), and 3) the salinity gradient across the ACC, which, while affected by variations in surface fresh water flux, seems largely determined by the rate and salinity of North Atlantic Deep Water upwelled on the poleward side of the ACC.

Of these three criteria, the atmospheric components of the models have a larger impact on the simulation of the winds and the gradient in surface heat flux across the current. The ocean components of the coupled models seem to largely determine the rate and salinity of NADW supplied to the Southern Ocean. In most models there is a significant disconnect between the rate of overturning in the North Atlantic and the amount of NADW-like water that is exported from the Atlantic into the Southern Ocean at 30°S. The best simulations of the strength and water mass characteristics of the ACC have a strong connection between the formation rate and the export rate of NADW in the South Atlantic (See Table 2).

Based on the analysis presented here, we find that we can divide the Southern Ocean simulations produced by the twelve models into five different classes. While these classes are derived from the IPCC AR4 model simulations of pre-industrial climate, we think they have a broader application. It is possible that some past (and future) climates may fall into these broad categories.

The results obtained from the three GISS models do not fit neatly into these categories or classes. As noted in the discussion in the previous sections, these models produce exaggerated thermal gradients across the ACC that compensate for extremely

weak or reversed salinity gradients. Given these particular simulation problems, it is hard to categorize the nature of the errors in any simple way. Therefore, we chose to exclude those model results in the classification exercise below.

1) To fall into the first simulation class, the "about right" scenario, a model must simulate the strength and position of the Antarctic Circumpolar for approximately the right reasons. The model must correctly simulate the magnitude and position of southern hemisphere westerly winds, the magnitude and distribution of heat and fresh water fluxes, as well as the heat and salt transport into the Southern Ocean associated with NADW. Only the GFDL-CM2.1 experiment falls into this category. It has its peak winds close to the observed latitude, a reasonable wind stress, fed with the right amount and type of NADW, resulting in near-observed ACC transport, as well as heat and fresh water fluxes.

2) The second class of Southern Ocean simulation falls short of the first classification primarily due to excessive wind stress over the ACC that leads to excessive ACC transport. The too strong ACC transport occurs for two reasons, the mechanical force imparted by the wind, and the excessive upwelling of saline NADW along the southern edge of the ACC. The CSIRO-Mk3.0, MIROC3.2 (medres) and MIROC3.2 (hires) simulations fall into this category (Figs 2 & 5). There are aspects of the UKMO-HadCM3 simulation that would fit into this category as well.

3) The third class of Southern Ocean simulation is characterized by an equatorward displacement of the peak wind stress over the Southern Ocean relative to observations while maintaining relatively strong winds over the channel. The strong winds drive strong subtropical gyres and boundary currents like the east-Australia Current and the Agulhas Current which inject both heat and salt into the surface waters of the ACC in the southwestern corners of the basins, weakening the density gradient across the channel and thus the ACC. The MIROC3.2 (hires) simulation suffers from this shortcoming as do the GFDL-CM2.0 and MRI-CGCM2.3.2a experiments.

4) In the fourth class of simulation, an equatorward wind shift is accompanied by weak winds over the channel. In this case, the injection of heat and salt from the subtropics into the Southern Ocean is substantially reduced and the Southern Ocean is dominated by very cold water adjacent to Antarctica, a very strong thermal gradient across the current, and an excessively strong ACC. The CNRM-CM3 simulation roughly

fits this type, although the ACC transport in the CNRM experiment seems severely restricted by the too shallow topography throughout the Southern Ocean (Fig. 3e). This regime reminds us of what was typical of simulations obtained from ocean-only models under restoring boundary conditions many years ago, when ocean-only models were often forced with the HR83 wind climatology (See Bryan and Lewis 1979 as an example). HR83 is known to be too weak and too equatorward (Harrison, 1989) and the use of restoring boundary conditions at the surface keeps the Polar and Subantarctic fronts at fixed locations, allowing cold water to collect on the south side of the ACC.

5) The fifth categorization criterion is related to the formation rate and density of the model's NADW. If NADW is excessively weak, fresh or warm, then it will not cross below the sill depth of the Drake Passage topographic features and upwell on the southern side of the ACC as in the observations. Weak and/or shallow NADW leads to a too weak eastward ACC transport as the density gradient across the current is smaller than observed (all other things being equal). Only the IAP-FGOALS1.0 and MRI-CGCM2.3.2a simulations fall into this class (Table 2). Conversely, too large southward NADW export below sill depth will lead to an exaggerated ACC as the saline NADW greatly increases the density of water adjacent to the Antarctic coast. Although the UKMO-HadCM3 simulation does have an exaggerated salinity gradient across the ACC and could fit in this category of simulation (See Fig 4), the salinity gradient is largely the result of a surface subtropical fresh water bias (See Fig 9, 12), rather than an excessive NADW upwelling component.

Increasing ocean stratification associated with global warming has been posited to serve as a positive feedback on global warming, reducing the oceanic uptake of anthropogenic carbon dioxide. Previous model results suggest that both the warming associated with anthropogenic CO_2 increase and the increased hydrological cycle could lead to a reduced oceanic uptake of anthropogenic CO_2 in the Southern Ocean, assuming small changes in biological activity. We expect that the differences in the Southern Ocean control climates indicated here will impact these models' responses to changes in radiative forcing with respect to heat and carbon dioxide uptake. This is the subject of a subsequent study.

6. Conclusions

The quality of a coupled climate model's Southern Ocean simulation depends upon both its atmospheric and ocean model components. These two model components influence each other in ways evident in the coupled system's air-sea momentum and buoyancy fluxes, and in the resulting three-dimensional Southern Ocean circulation. Away from the surface, in the ocean interior, the mixing of different water masses largely determines the properties of the water that is upwelled to the surface at a rate that in turn is influenced by winds. And since air-sea heat fluxes over the vast Southern Ocean impact the surface climate within and beyond the Southern Ocean region, a global coupled model's Southern Ocean simulation affects the model's mean climate as well as its response to transient forcings, such as those associated with climate change scenarios. With so many interconnected pieces, it is a challenge to get the Southern Ocean "right" in a global coupled climate model.

In the set of coupled climate models presented here, we find that the most important gauges for assessing the likely Southern Ocean simulation performance, in descending order of importance, are 1) the strength of the westerly wind over the Drake Passage latitude band, 2) the heat flux gradient over the same latitude band (although this quantity is relatively well simulated by the models presented here and therefore introduces little of the inter-model differences presented here), and 3) the salinity gradient across the ACC, which, while affected by variations in surface fresh water flux, seems largely determined by the rate and salinity of North Atlantic Deep Water upwelled on the poleward side of the ACC. Additional factors found to influence some Southern Ocean simulations include the latitudinal location of the westerly winds and a model's Southern Ocean bathymetry.

Based upon these criteria, a framework for categorizing a model's Southern Ocean simulation has been developed and applied to a set of coupled climate models associated with the forthcoming IPCC Fourth Assessment Report. Only one of the 12 models examined is found to have a Southern Ocean simulation that is not considerably deficient with regard to at least one of the criteria used in this study. Eight other models are categorized according to which of the criteria they fail to meet, providing information

about how and why those model's Southern Ocean simulations differ markedly from observations.

Acknowledgements

We acknowledge the international modeling groups for providing their data for analysis, the Program for Climate Model Diagnosis and Intercomparison (PCMDI) for collecting and archiving the model data, the JSC/CLIVAR Working Group on Coupled Modeling (WGCM) and their Coupled Model Intercomparison Project (CMIP) and Climate Simulation Panel for organizing the model data analysis activity, and the IPCC WG1 TSU for technical support. The IPCC Data Archive at Lawrence Livermore National Laboratory is supported by the Office of Science, U.S. Department of Energy. We thank Anand Gnanadesikan and Mike Winton for thoughtful reviews and discussions.

References

Bryan, K., and L. J. Lewis, 1979: A water mass model of the world ocean. *Journal of Geophysical Research,* **84(C5),** 2503-2517.

Cubasch, U., G. A. Meehl, G. J. Boer, R. J. Stouffer, M. Dix, A. Noda, C. A. Senior, S. Raper, K. S. Yap, A. Abe-Ouchi, S. Brinkop, M. Claussen, M. Collins, J. Evans, I. Fischer-Bruns, G. Flato, J. C. Fyfe, A. Ganopolski, J. M. Gregory, Z.-Z. Hu, F. Joos, T. Knutson, R. Knutti, C. Landsea, L. Mearns, C. Milly, J. F. B. Mitchell, T. Nozawa, H. Paeth, J. Räisänen, R. Sausen, S. Smith, T. Stocker, A.Timmermann, U. Ulbrich, A. Weaver, J. Wegner, P. Whetton, T. Wigley, M. Winton, and F. Zwiers, 2001: **9. Projections of future climate change**. In *Climate Change 2001: The Scientific Basis. Contribution of Working Group I to the Third Assessment Report of the Intergovernmental Panel on Climate Change*, Cambridge, UK: Cambridge University Press, 526-582.

da Silva, A.M., C.C. Young and S. Levitus, 1994: Atlas of Surface Marine Data 1994 Volume 1: Algorithms and Procedures. In: NOAA Atlas NESDIS (6) . U.S. Department of Commerce, Washington D. C., **83**.

Gent, P.R., W.G. Large and F.O. Bryan, 2001: What sets the mean transport through Drake Passage? *J. Geophys. Res.*, **106**, 2693-2712.

Gille, S. T., 1997. The Southern Ocean Momentum Balance: Evidence for Topographic Effects from Numerical Model Output and Altimeter Data, *J. Phys. Oceanogr.*, **27**, 2219-2232

Gnanadesikan, A. and R. Hallberg, 2000: On the relationship of the circumpolar current to Southern Hemisphere winds in large-scale ocean models. *J. Phys. Oceanogr.*, **30**, 2013-2034.

Gordon, A. L., 1971. Oceanography of Antarctic waters, in *Antarctic Oceanology I*: J. L. Reid, ed., Antarctic Research Series, Washington, D.C., American Geophysical Union, p. 169-203.

Harrison, D.E., 1989: On climatological monthly mean wind stress and wind stress curl fields over the World Ocean. *J. Climate*, **2**(1), 57 - 70.

Hellerman, S. and M. Rosenstein, 1983. Normal monthly wind stress over the world ocean with error estimates. *J. Phys. Oceanogr.*, **13**, 1093-1104

Manabe, S., R. J. Stouffer, M. J. Spelman, and K. Bryan, 1991: Transient responses of a coupled ocean-atmosphere model to gradual changes of atmospheric CO2. Part I: Annual mean response**.** *J. Climate,* **4**, 785-818.

McCartney, M.S., 1977. Subantarctic Mode Water. In: *A Voyage of Discovery: George Deacon 70th Anniversary Volume*, M. V. Angel, editor, Supplement to Deep-Sea Research, Pergamon Press, Oxford, pp. 103-119.

McCartney, M.S., 1982. The subtropical recirculation of Mode Waters. *Journal of Marine Research*, **40**, suppl., 427-464.

Munk, W.H. and E. Palmen, 1951: Note on the dynamics of the Antarctic Circumpolar Current. *Tellus*, **3**, pp. 53-55.

Nowlin, W.D., Jr. and J.M. Klinck, 1986: The Physics of the Antarctic Circumpolar Current. *Rev. Geophys.*, **24**, 469-491.

Peterson, R.G. and T. Whitworth III, 1989: The subantarctic and polar fronts in relation to deep water masses through the southwestern Atlantic. *J. Geophys. Res.*, **94**, 10,817-10,838.

Sarmiento, J.L., T.M.C. Hughes, R.J. Stouffer, and S. Manabe, 1998: Simulated response of the ocean carbon cycle to anthropogenic climate warming. *Nature*, **393(6682)**, 245-249.

Schmitz, W.J., 1996, On the World Ocean Circulation: Volume I. Some Global Features/North Atlantic Circulation. *Woods Hole Oceanographic Institution Technical Report*, WHOI-96-03, 141 pp.

Schulman, E.E., 1975: A study of topographic effects. In: *Numerical Models of Ocean Circulation*, National Academy of Science, Washington, D.C., 147-16

Stevens, D.P. and V.O. Ivchenko, 1997: The Zonal Momentum Balance in an Eddy Resolving General Circulation Model of the Southern Ocean. *Quarterly Journal of the Royal Meteorological Society*. **123**, 929-951.

Stommel, H., 1957: A survey of ocean current theory. *Deep Sea Research,* **4***,* 149-84.

Stouffer, R.J., and K.W. Dixon, 1998: Initialization of coupled models for use in climate studies: A review. In *Research Activities in Atmospheric and Oceanic Modelling*, Report No. 27, WMO/TD-No. 865, World Meteorological Organization, Geneva, Switzerland, I.1-I.8.

Stouffer, R.J., A. J. Weaver, and M. Eby, 2004: A method for obtaining pre-twentieth century initial conditions for use in climate change studies. *Climate Dynamics*, **23**, 327-339.

Talley, L.D., 1996: Antarctic Intermediate Water in the South Atlantic. In *The South Atlantic: Present and Past Circulation*, G. Wefer et al., Eds., Springer-Verlag, 219–238.

Talley, L.D., 1999: Some aspects of ocean heat transport by the shallow, intermediate and deep overturning circulations. *Mechanisms of Global Climate Change at Millennial Time Scales*, Geophys. Monogr., **Vol. 112**, Amer. Geophys. Union, 1–22.

Talley, L. D., 2003. Shallow, intermediate and deep overturning components of the global heat budget. *J. Phys. Oceanogr.*, **33**, 530-560.

Taylor, K. E., D. Williamson, and F. Zwiers, 2000: The sea surface temperature and sea-ice concentration boundary conditions for AMIP II Simulations, PCMDI Report No. 60, UCRl-JC-125597

Trenberth, K. E., and J. M. Caron, 2001: Estimates of meridional atmosphere and ocean heat transports. *J. Climate.*, **14**, 3433-3443.